Modeling the Recent Evolution of Global Drought and Projections for the Twenty-First Century with the Hadley Centre Climate Model

ELEANOR J. BURKE, SIMON J. BROWN, AND NIKOLAOS CHRISTIDIS

Hadley Centre for Climate Prediction and Research, Met Office, Exeter, United Kingdom

ABSTRACT

Meteorological drought in the Hadley Centre global climate model is assessed using the Palmer Drought Severity Index (PDSI), a commonly used drought index. At interannual time scales, for the majority of the land surface, the model captures the observed relationship between the El Niño–Southern Oscillation and regions of relative wetness and dryness represented by high and low values of the PDSI respectively. At decadal time scales, on a global basis, the model reproduces the observed drying trend (decreasing PDSI) since 1952. An optimal detection analysis shows that there is a significant influence of anthropogenic emissions of greenhouse gasses and sulphate aerosols in the production of this drying trend. On a regional basis, the specific regions of wetting and drying are not always accurately simulated. In this paper, present-day drought events are defined as continuous time periods where the PDSI is less than the 20th percentile of the PDSI distribution between 1952 and 1998 (i.e., on average 20% of the land surface is in drought at any one time). Overall, the model predicts slightly less frequent but longer events than are observed. Future projections of drought in the twenty-first century made using the Special Report on Emissions Scenarios (SRES) A2 emission scenario show regions of strong wetting and drying with a net overall global drying trend. For example, the proportion of the land surface in extreme drought is predicted to increase from 1% for the present day to 30% by the end of the twenty-first century.

1. Introduction

Drought is amongst one of the world's costliest disasters and affects a very large number of people every year (Wilhite 2000). A drought is considered to be a period of abnormally dry weather that causes serious hydrological imbalance in a specific region. However, the definitions of "serious" and "abnormally dry" depend on the extent and nature of the impact of the drought on the local society. It is important to monitor drought events and their variability, explore their predictability, and determine how they might change under future climate scenarios.

Global circulation models (GCMs) have been used previously to investigate water availability. For example, Gregory et al. (1997) used detailed knowledge of the GCM-simulated hydrology to study summer drought in continental midlatitudes and suggested that, in the future, there is a greater likelihood of long dry spells caused by a tendency toward fewer precipitation

Corresponding author address: Dr. Eleanor Burke, Hadley Centre for Climate Prediction and Research, Met Office, FitzRoy Road, Exeter, EX1 3PB, United Kingdom.
E-mail: eleanor.burke@metoffice.gov.uk

events rather than less precipitation. Wetherald and Manabe (2002) and Manabe et al. (2004) showed a global increase in runoff rate under future climate scenarios. They also found reduced soil moisture in semi-arid regions, and, in Northern Hemisphere middle and high latitudes, increased soil moisture in the winter and decreased soil moisture in the summer.

There are many quantitative definitions of drought based upon knowledge of precipitation, soil moisture, potential evapotranspiration, or some combination thereof (Heim 2002; Wilhite and Glantz 1985; World Meteorological Organization 1975; Svoboda et al. 2002). These drought indices all have their own advantages and disadvantages (Keyantash and Dracup 2002). The Palmer Drought Severity Index (PDSI; Palmer 1965) is a commonly used and widely accepted meteorological drought index (e.g., Cook et al. 1999; Dai et al. 2004; Lloyd-Hughes and Saunders 2002; Ntale and Gan 2003; Shabbar and Skinner 2004; http://nadss.unl.edu). It is obtained from a simplistic model of the cumulative anomaly of moisture supply and demand at the land surface, which requires knowledge of both precipitation and potential evapotranspiration.

Rind et al. (1990) and Jones et al. (1996) compared the PDSI, calculated using data from a GCM, with ob-

servations over North America and Europe. They projected that, by the middle of the twenty-first century, severe drought will occur a large proportion of the time. However, their calculation of the PDSI uses a parameterization of potential evaporation based only on temperature and latitude (Thornthwaite 1948). This parameterization overestimates the increase in potential evapotranspiration in the future and hence the drying (Lockwood 1999).

Recently, global estimates of the PDSI have been prepared (Dai et al. 2004) using observed temperature and precipitation data. This paper uses these data as a basis for evaluating the ability of the Third Hadley Center Climate Model (HadCM3) to predict present-day drought events on a global basis. First, it compares global variations in the modes of variability of the estimated and modeled PDSI. Then it assesses how well the model predicts the frequency, duration, and spatial extent of global drought events (defined by a low PDSI value). The suitability of an alternative parameterization of the potential evaporation, the Penman–Montheith equation (Shuttleworth 1993), for calculating the PDSI under future climates was demonstrated. Finally, future projections of the PDSI and associated global drought events were assessed using time-dependent climate change experiments based on the Intergovernmental Panel on Climate Change (IPCC) Special Report on Emissions Scenarios (SRES) A2 (Nakicenovic et al. 2000).

2. Models and data

a. PDSI

The PDSI was created by Palmer (1965) to provide the "cumulative departure of moisture supply." Full details of the calculation of the PDSI can be found at the National Agricultural Decision Support System (http://nadss.unl.edu). The PDSI is a hydrologic accounting scheme that uses a simple two-layer, bucket-type land surface scheme to partition the incoming precipitation into the components of the water balance. It was developed using limited data from the central United States. To compare it across space and time, the components of the water balance were calibrated by climatologically appropriate values for the specific time of year and location. When using the PDSI to explore the changes in wetness and dryness as a result of future climate scenarios, these calibration factors were held at the present-day values (Rind et al. 1990).

Critics of the PDSI (e.g., Alley 1984) suggest that it is of insufficient complexity to account accurately for the wide range of environmental conditions that may in reality occur such as frozen soil, snow, and the presence of roots or vegetation. Therefore the calculated soil moisture is inferior and should not be used as a measure of hydrological drought. However, since the PDSI was developed to provide a measure of meteorological drought these issues are less significant. Despite trying to normalize for location and season, the PDSI is not spatially comparable across the contiguous United States (Guttman et al. 1992). Therefore quantitative interpretations of dryness or wetness for a given PDSI value depend on local mean climate conditions. This was taken into consideration in the global assessment of the PDSI and the definition and evaluation of drought events.

An estimate of the potential evapotranspiration (E_p) is key in calculating the PDSI. The Thornthwaite (1948) method, based on knowledge of the temperature and latitude, is traditionally used to calculate E_p in the PDSI. This calculation implicitly assumes some form of correlation between potential evapotranspiration, temperature, and the shortwave radiation at each latitude. Under future climate scenarios the temperature is predicted to increase while shortwave radiation is relatively independent of climatic effects. Therefore, the present-day link between temperature and latitude and shortwave radiation will be altered (Lockwood 1999). If the temperature at a specific latitude increases in the future, the Thornthwaite (1948) algorithm will overestimate the potential evaporation because it overestimates the solar radiation (Lockwood 1999). This results in an unrealistic increase in drought frequency. Therefore the Penman–Montheith equation (Shuttleworth 1993) is a more appropriate method of calculating E_p. In this paper the Penman–Montheith potential evapotranspiration (in mm day^{-1}) E_p is given by

$$E_p = \frac{\Delta}{\Delta + \gamma} R_n + \frac{\gamma}{\Delta + \gamma} \frac{6.43(1 + 0.536U)D}{\lambda}, \quad (1)$$

where R_n is the net radiation in mm day^{-1}, U is the wind speed in m s^{-1} measured at 2-m height, λ is the latent heat of vaporization of water in MJ kg^{-1}, D is the vapor pressure deficit in kPa, Δ is the slope of the relationship between saturated vapor pressure and temperature in kPa K^{-1}, and γ is the psychrometric constant in kPa K^{-1}. Limited global observational data restricts the use of the Penman–Montheith equation to GCM output. Therefore, in this paper, two versions of the PDSI were calculated, the first using the Thornthwaite equation (PDSI-T) and the second using the Penman–Montheith equation (PDSI-PM). The equivalence of these two calculations is demonstrated for present-day climates. PDSI-T was used for comparing with observations and PDSI-PM for assessing future climate change.

The global PDSI calculated by Dai et al. (2004) is available from 1870 to 2002 (http://www.cgd.ucar.edu/cas/catalog/climind/pdsi.html). Dai et al. (2004) used observations of monthly surface air temperature and precipitation to calculate the PDSI at a resolution of 2.5° by 2.5°. The PDSI data calculated from observations for the period between 1952 and 1998 were used in this study (OBS hereafter). For comparison purposes they were regridded to the resolution of the model atmosphere (3.75° by 2.5°). The restricted time period was selected to ensure a temporally consistent missing data mask—any grid cell with any missing data during that time period was excluded—and to ensure a consistent overlap with the relevant model integrations.

b. Hadley Centre climate model

This paper is mainly based on results from integrations of HadCM3, the third version of the Hadley Centre coupled ocean–atmosphere GCM (Gordon et al. 2000). The model has a resolution of 3.75° by 2.5° (19 levels) for the atmosphere. It requires no adjustment of the heat fluxes at the ocean–atmosphere interface. A full range of physical parameterizations are included consistent with a state-of-the-art coupled general circulation model.

The first simulation analyzed is a 2000-yr control integration (CTL) of the coupled model, HadCM3, with fixed external forcing, representing preindustrial levels of greenhouse gases. The climate is realistic and stable (Johns et al. 2003). This long-time-scale integration is used to determine the modeled internal climatic variability.

To perform a direct comparison with available observations, coupled HadCM3 simulations with realistic twentieth-century external forcing were analyzed (ALL-C). Four ensemble members were available and are identical except for their initial conditions (Tett et al. 2002). The initial conditions were taken from states of the HadCM3 control run (CTL) separated by 100 yr. These simulations evolved their own sea surface temperature fields. Three of these were extended to 2100 using the IPCC SRES A2 emission scenario (Nakicenovic et al. 2000) in order to produce projections of climate over the twenty-first century (A2; Johns et al. 2003).

A second six-member ensemble was created from 1946 to 2002 with just the atmospheric component of the coupled model (HadAM3; Pope et al. 2000) forced with all known external forcings (ALL-A) as part of the Climate Variability and Predictability Study (CLIVAR) International Climate of the Twentieth Century Project (Folland et al. 2002). These simulations were driven by the observed sea surface temperature fields (HadISST) of Rayner et al. (2003).

To compare the model and observations, PDSI-T was calculated using the monthly precipitation and air temperature fields from the CTL and present-day (ALL-A and ALL-C) integrations. Soil water holding capacities were taken from the Webb et al. (1993, 2000) dataset used by Dai et al. (1998, 2004). The preset-day integrations were calibrated in the same way as the observations with climatologically appropriate values of the components of the water balance (calibration factors) calculated for each ensemble member using data between 1950 and 1979. Calibration factors for CTL were calculated using the entire 2000-yr integration. Penman–Montheith potential evapotranspiration was calculated using monthly modeled net radiation, air temperature, wind speed, relative humidity, and pressure and used to calculate PDSI-PM for the CTL and ALL-A simulations and for the assessment of future climate scenarios.

3. Present-day variability of PDSI-T

Monthly PDSI-T calculations were used to compare the model integrations with observations. Interannual variability (covering time scales between 18 months and 8 yr) in PDSI-T was explored independently to lower-frequency variability (time scales greater than 8 yr) to separate the changes associated with phenomena such as the El Niño–Southern Oscillation (ENSO) from any longer-term changes. These two time scales were extracted using the digital filter of Walraven (1984). Modes of global interannual variability were calculated using standard empirical orthogonal function (EOF) covariance analysis. All resultant EOF spatial fields or eigenvectors were scaled so that their amplitude is equal to the square root of their eigenvalue. In addition, the time series or principal components (PCs) corresponding to each EOF were scaled to have unit variance. The eigenvectors and PCs obtained after a Varimax rotation of the reconstructed field (including 70% of the variance) were found to be essentially the same as for the unrotated case. Therefore, results shown here represent an unrotated EOF analysis. Low-frequency variability was explored using a trend analysis of the filtered PDSI.

a. Interannual variability of PDSI-T

At interannual time scales the first EOF of PDSI-T accounts for approximately 10% of the variability in both model and observations. In general, there is good agreement between the three sets of model integrations (ALL-A, ALL-C, and CTL) and the OBS, with the
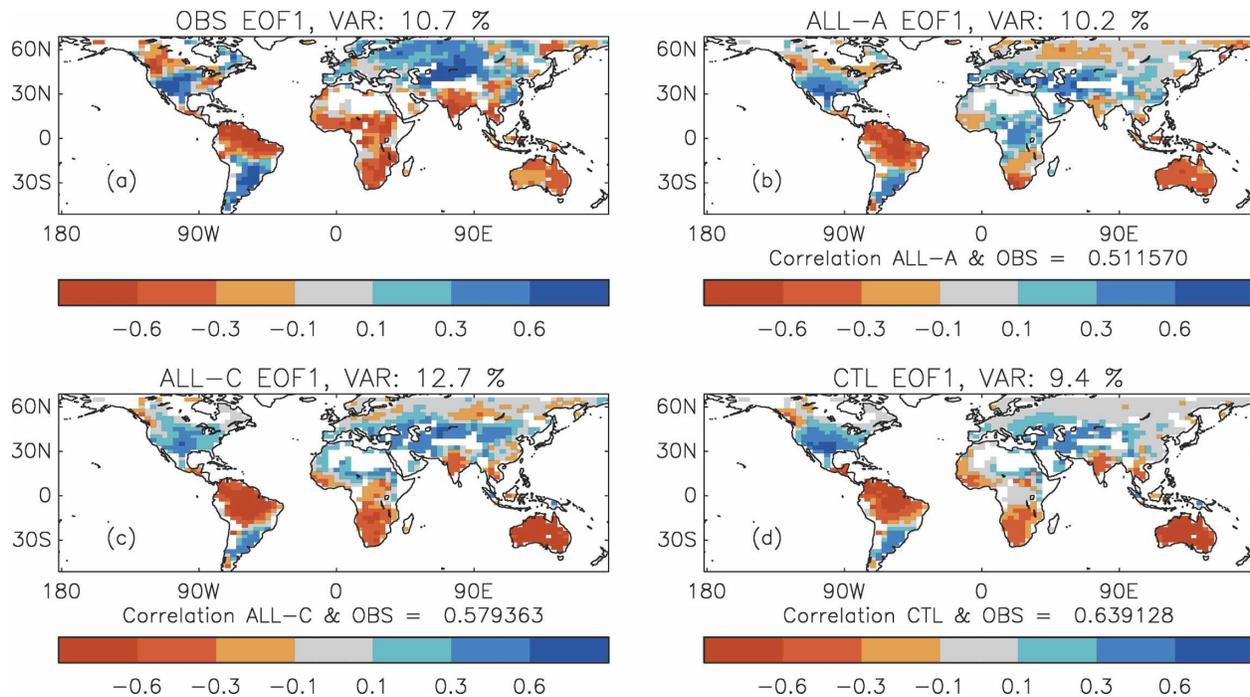
FIG. 1. The spatial patterns of the leading EOFs of the filtered PDSI with all time scales between 18 months and 8 yr included for (a) OBS; (b) ALL-A; (c) ALL-C; and (d) CTL.

area-weighted spatial correlations ranging from 0.51 to 0.64 (Fig. 1). The model integrations show a negative signal over Australia, southern Africa, India, and Amazonia together with positive signals over the United States and much of Europe and central Asia. These features represent the features seen in the OBS, although the positive signal in the United States is more widespread in the model integrations and misses the relative drying on the east coast. The positive signal over Eurasia extends farther north in the OBS than in the model integrations. Spatial correlation coefficients between ALL-A and OBS are 0.27, 0.31, 0.45, 0.70, and 0.31 for Australia, southern Africa, Amazonia, United States, and Europe, respectively. There are some noticeable differences between the models and OBS over the Sahel and central Africa.

Figure 2 shows the first principal component (PC1) of PDSI-T for the observations and the model integrations: ALL-A, ALL-C, and CTL (in the case of the CTL only a representative period is shown). Also shown are the corresponding Niño-34 indices shifted forward in time by six months and filtered to retain the same time scales as the PDSI. The observed Niño-34 indices were obtained from the National Weather Service Climate Prediction Center (http://www.cpc.ncep. noaa.gov/data/indices/). The Niño-34 indices for the coupled model are the standardized anomaly of the area-average temperature for the region 5°N–5°S and

170°–120°W. The correlation between ALL-A PDSI-T PC1 and the observed Niño-34 indices produced coefficients ranging between 0.75 and 0.86 (Fig. 2a), which compares favorably with the OBS correlation of 0.85. The ALL-C correlation coefficients are 0.85, 0.77, 0.54, and 0.75 using the modeled Niño-34 index and 0.76 for 150 yr of the CTL integration (Figs. 2b–f). Therefore, on a global basis, the model reproduces the joint ENSO and PDSI variability observed by Dai et al. (1998, 2004).

b. Low-frequency variability of the PDSI

The presence of any long-term changes in the observed PDSI was assessed using a trend analysis. PDSI-T was filtered so as to retain information for time scales greater than 8 yr. Figure 3 shows the spatial patterns generated following a point-by-point trend analysis of PDSI-T for the present day. There are areas of both drying and wetting but with an overall global drying. The greatest drying in the OBS is in the Sahel, southern Africa, and eastern Asia with regions of wetting in the United States, central Africa, western Australia, and central Asia (Dai et al. 2004). ALL-A captures many of these features (Fig. 3b) but with some areas of disagreement, including South America (too dry), Europe (too wet), and central-eastern Australia (too dry). Consequently the area-weighted spatial correlation with OBS is 0.35. On a regional basis the
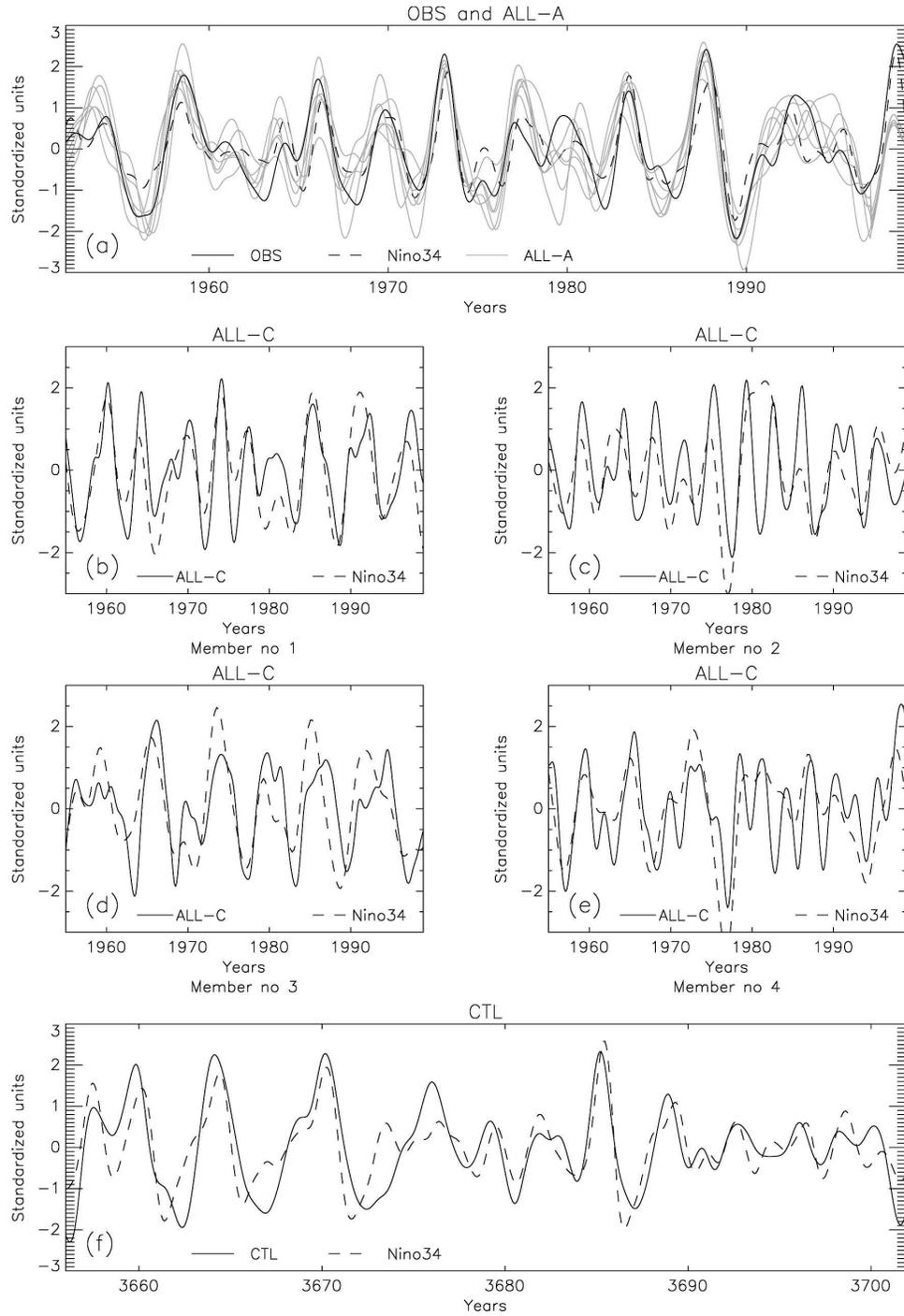
FIG. 2. The time series associated with the first EOF (PC1) of the filtered PDSI (with all time scales between 18 months and 8 yr included) and the PC1 of the filtered Niño-34 index (with all time scales between 18 months and 8 yr included) shifted to the right by 6 months. These time series are associated with (a) OBS and the six-member ensemble of ALL-A; (b)–(e) the four member ensemble of ALL-C; and (f) CTL.
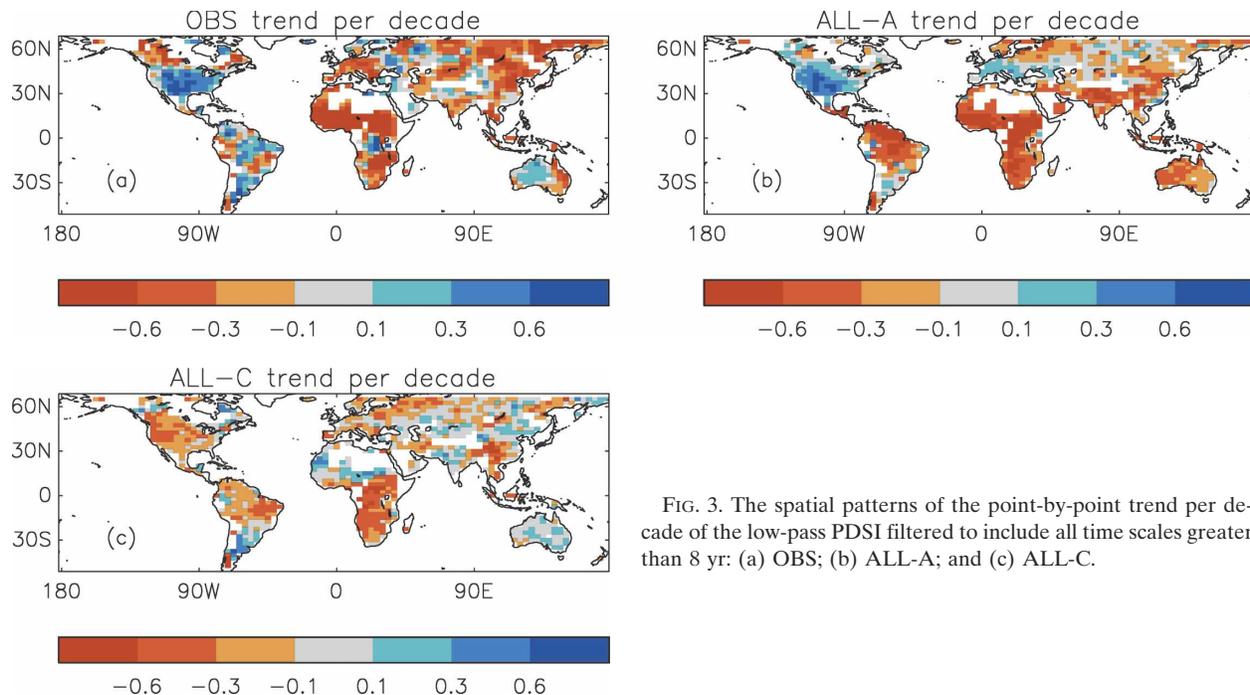
FIG. 3. The spatial patterns of the point-by-point trend per decade of the low-pass PDSI filtered to include all time scales greater than 8 yr: (a) OBS; (b) ALL-A; and (c) ALL-C.

changes observed in the United States, the Sahel, southern Africa, eastern Australia, and northern and western Eurasia are well represented by ALL-A with spatial correlation coefficients of 0.75, 0.56, 0.41, 0.37, and 0.44, respectively.

ALL-C (Fig. 3c) captures less of the observed pattern than ALL-A. Unlike ALL-A, the ALL-C ensemble members evolve independent sea surface temperatures so will contain uncorrelated contributions of natural variability; thus discrepancies between OBS and ALL-C and between the ALL-C ensemble members are likely to be much greater. The changes in the OBS that are captured by ALL-A but not by ALL-C are therefore likely to be due to natural or internal variability of the climate system, whereas those that are common between OBS, ALL-A, and ALL-C are more likely to be due to common external forcings.

Despite differences between the OBS and the model on a regional basis, Fig. 4 shows that ALL-A, ALL-C, and the OBS all produce a global drying trend between 1952 and 1998. Least squares linear regression shows the globally averaged OBS PDSI reducing by 0.25 decade^{-1} (Fig. 4a). ALL-A captures this change with trends ranging between −0.2 and −0.3 decade^{-1}. In the case of the ALL-C ensemble (Figs. 4b–e) the PDSI-T also decreases but by a smaller amount (−0.16, −0.12, −0.13, −0.06 decade^{-1}) than those in Fig. 4a. This reproduction of the observed trend is encouraging and provides some justification for using HadCM3 to assess future drought risk on a global scale. Figure 4 also indicates that there is multidecadal variability in the observed PDSI that is not captured in ALL-A, but is present in two of the ALL-C members (Figs. 4c and 4d). This suggests there may be coupled modes of internal variability on multidecadal time scales.

The significance of the drying trends is addressed using the 2000-yr control run, which has a stable climate (Johns et al. 2003) and gives information on the natural variability within the model. Running blocks of 47 yr were extracted from the 2000-yr CTL simulation and the magnitude of the trend in PDSI-T (filtered to remove time scales less than 8 yr) calculated for each of the blocks. Figure 5 shows the cumulative distribution function of these trends. Also shown are the trends in the observations, ALL-A, and ALL-C from Fig. 4. The trend in both the OBS and ALL-A is greater than the maximum trend found within the CTL. This suggests that these trends cannot be explained by the natural variability produced by the coupled model. In addition, for three of the four members of the ALL-C ensemble, there is a less than 1% chance that the trends found in ALL-C occurred as a result of natural variability alone. For the other member there is a 10% chance that the trend is as a result of natural variability. Therefore in the case of both ALL-A and ALL-C the trends are likely to be a result of external forcings on the climate system not present in the CTL simulation. This was explored further using an optimal detection analysis.
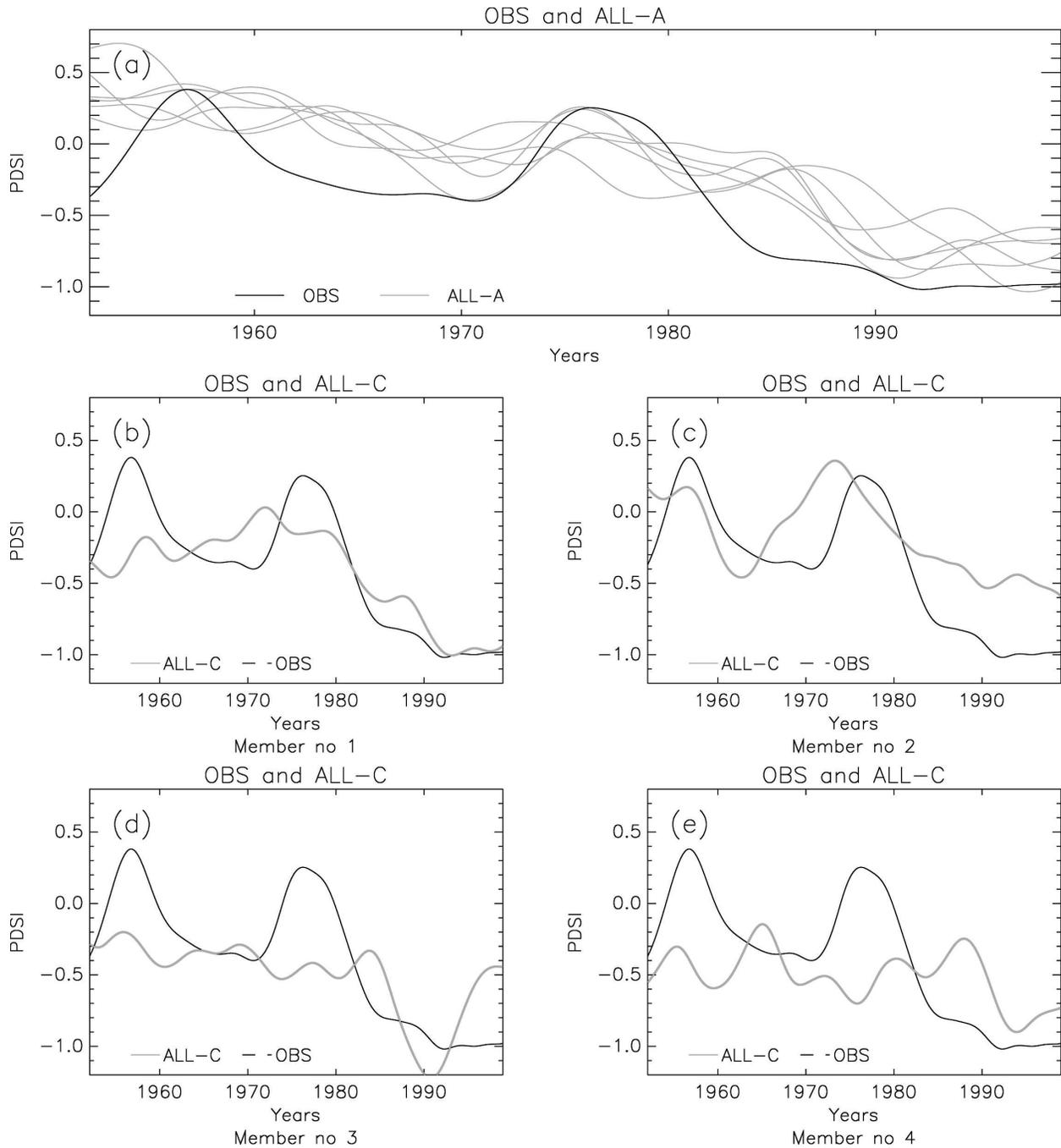
FIG. 4. The globally averaged PDSI filtered to include all time scales greater than 8 yr. The time series are associated with (a) OBS and the six members of ALL-A in gray and (b)–(e) OBS and the four members of ALL-C.

OPTIMAL DETECTION ANALYSIS OF PDSI TRENDS

The trend patterns found for the OBS and the ALL-C ensemble were compared in an optimal detection analysis, a formal statistical methodology that is widely used in the detection of a climate change signal and its attribution to external forcings [International ad hoc Detection and Attribution Group (IDAG) 2005]. The scaling factors required to match the model pattern (ensemble mean of ALL-C) with the observations (OBS) were estimated using a generalized multivariate regression, taking into account an estimate of the mod-
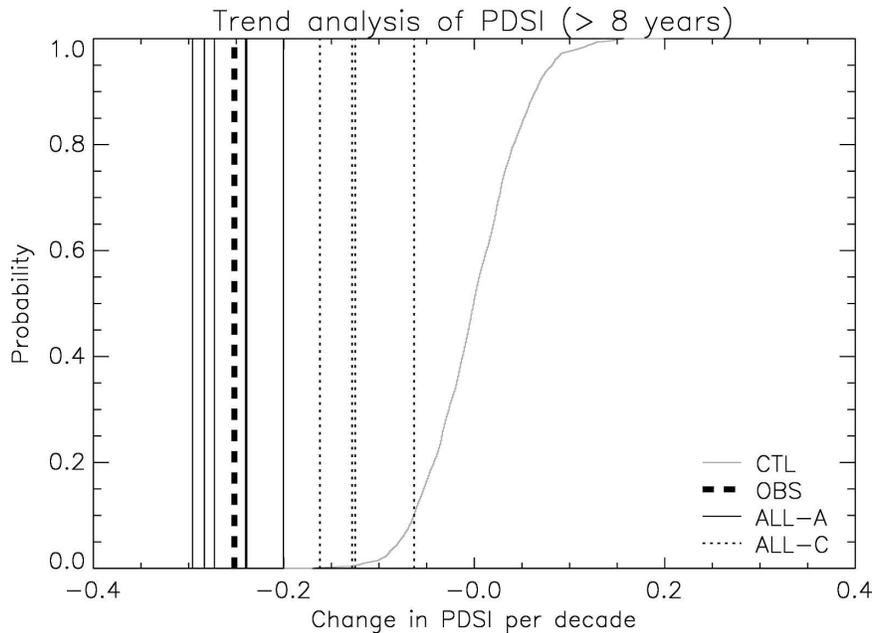
FIG. 5. The trend of the globally averaged PDSI calculated over 47-yr blocks using data that have been filtered to include all time scales greater than 8 yr. The cumulative distribution of the CTL simulation was calculated using running blocks. Also shown are the OBS, ALL-A, and ALL-C.

eled internal climate variability (CTL). The uncertainty in the scaling factors and the covariance matrix of the internal climate variability were computed using 58 segments (30 nonoverlapping) from 1800 yr of the CTL simulation. Scaling factors consistent with unity that have a small uncertainty range imply a good match between model and observations with a detectable signal whereas those consistent with zero imply no detection. The analysis was performed in the space defined by the 20 leading eigenvectors of the noise covariance, and is generally stable for truncations in the same vicinity or higher. Full details of the statistical model used are given by Allen and Stott (2003).

The best estimate of the scaling factor is 2.66. This is higher than unity, implying that the model patterns need to be scaled up to agree with the OBS. This suggests that the ALL-C ensemble underestimates the trends found in the OBS. The 5% to 95% uncertainty range on this scaling factor is between 1.55 and 5.06. Since the zero value falls outside this range, it can be concluded that significant changes in the observed PDSI as a result of external forcings are detectable.

c. Drought events

Droughts were identified using critical values of the PDSI defined (independently for each grid cell) as the 20th percentile of the PDSI distribution for that grid cell. On average, the limiting value for the 20th percentile of the PDSI is -2.0. The PDSI distribution was obtained from the time series of monthly PDSI between 1952 and 1998 smoothed using an 18-month running mean. On average, at any one time 20% of the land surface will be in drought. This method of defining drought events helps eliminate biases between model, observations, and locations. Figures 6a and 6b show the proportion of the land surface in drought for OBS, ALL-A, and ALL-C. Over the time period shown OBS shows an increase in the percentage of the land surface in drought by 3.4% decade^{-1} and ALL-A by between 2.9% and 4.6% decade^{-1}. Over the longer time period between 1905 and 1998 ALL-C shows an increase of between 0.5% and 0.9% decade^{-1}. In all cases the majority of this change occurs in the 1980s and 1990s.

Drought events are defined as the continuous periods of time (greater than or equal to 1 month) where the PDSI is less than the critical value for the grid cell. Figure 7 shows the mean number of events over the land surface and their mean duration. In the case of OBS, ALL-A, and ALL-C they were calculated for the period 1952–98 and each ensemble member is shown separately. To represent the natural variability within the model, the CTL integration was divided into blocks of consecutive 47-yr periods and the calculations made for each block. Figure 7 shows that all the forced model

Proportion land in drought
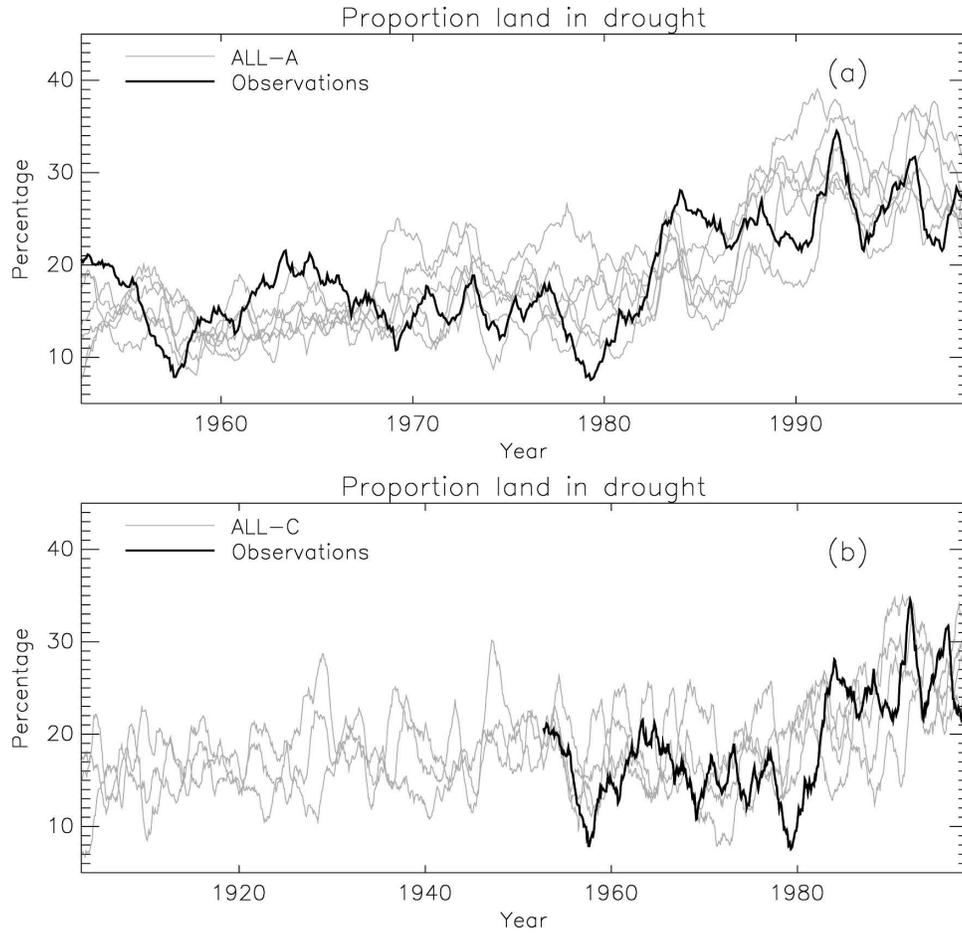

Proportion land in drought

FIG. 6. The proportion of the land surface in drought at each time step for (a) ALL-A and OBS and (b) ALL-C and OBS. Drought is defined as the 20th percentile of the entire PDSI time series.

simulations fall within the natural variability of the CTL simulation. ALL-C falls within one standard deviation of the mean of the CTL distribution and ALL-A falls within two standard deviations. However, OBS falls outside the variability of the model—OBS has ap-

proximately 2 more events per 100 yr than the model predicts. In addition, the model predicts longer events of between 21- and 26-months duration compared with the OBS, which predicts average event durations of 19 months.
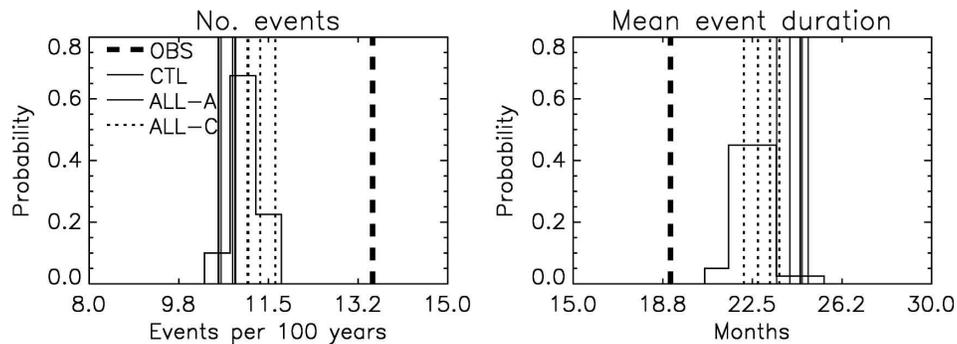

FIG. 7. (a) The mean number of events per 100 yr and (b) the mean event duration over the land surface.
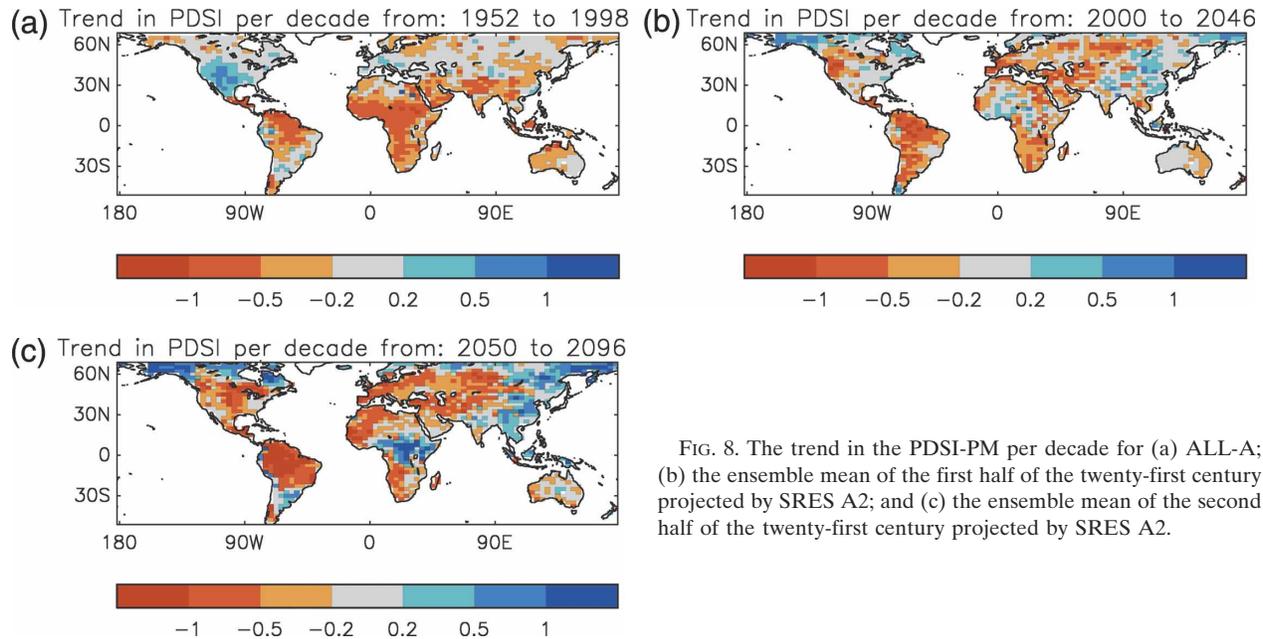
FIG. 8. The trend in the PDSI-PM per decade for (a) ALL-A; (b) the ensemble mean of the first half of the twenty-first century projected by SRES A2; and (c) the ensemble mean of the second half of the twenty-first century projected by SRES A2.

4. Future projections of drought

More realistic future projections of drought are obtained using the PDSI-PM [calculated using the Penman–Montheith potential evapotranspiration—Eq. (1)] instead of the PDSI-T. The impact of this change on the resultant PDSI values calculated using preindustrial data (CTL) was minimal. For both of the time scales under discussion area-weighted spatial correlation coefficients between the first EOF spatial patterns of PDSI-T and PDSI-PM for the CTL are greater than 95% and correlations between the first principal components are greater than 96%.

The spatial distribution of changes in the PDSI over the twenty-first century was explored by calculating the trend in the PDSI-PM per decade at each point using the A2 ensemble (Fig. 8). The variability between the three A2 ensemble members is small with consistent projections between the members. The model predicts drying over Amazonia, the United States, northern Africa, southern Europe, and western Eurasia, and wetting over central Africa, eastern Asia, and high northern latitudes. [Note: Fig. 3 shows some regional discrepancies between model and observations; therefore regional changes must be assessed with care.] There is an overall drying trend with a decrease in the global average PDSI of 0.30 decade^{-1} projected for the first half of the twenty-first century. This is of similar magnitude to the decrease in the present-day PDSI-PM, represented by the ALL-A model integrations (0.39 decade^{-1}). The rate of drying over the second half of the

twenty-first century increases, with the PDSI-PM decreasing by 0.56 decade^{-1}.

Figure 9 shows the projected increase in the proportion of the land area under drought over the twenty-first century. As before, the 20th percentile of the present-day (1952–98) PDSI-PM distribution defines moderate drought. In addition, the 1st and 5th percentiles of the present-day PDSI-PM distribution define two more levels of drought (extreme and severe drought respectively). On average the limiting PDSI values for extreme, severe, and moderate drought are −4.3, −3.3, and −2.0, respectively. Figure 6 shows that the percentage of the land surface in drought had increased by the beginning of the twenty-first century from 1% to 3% for the extreme droughts, from 5% to 10% for the severe droughts, and from 20% to 28% for the moderate droughts. This increase continues throughout the twenty-first century (Fig. 9) and by the 2090s the percentage of the land area in drought increases to 30%, 40%, and 50% for extreme, severe, and moderate drought, respectively. [Note: if PDSI-T were used the proportion of the land in drought at the end of the twenty-first century is predicted to be 65%, 75%, and 85%, respectively.]

Table 1 shows the number of drought events (defined as before) per 100 yr and their mean duration for the three categories of droughts. In all cases, as the severity of drought increases, the number of drought events and the duration of each decreases. In the future, for extreme and severe drought the number of drought events is projected to double, while for moderate
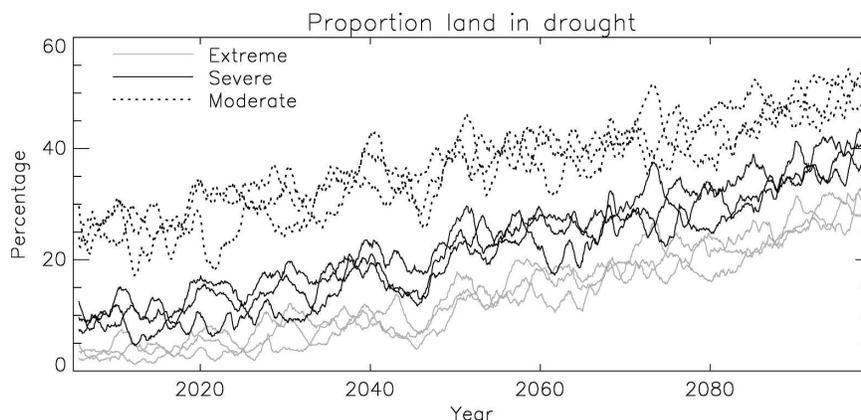
FIG. 9. The proportion of the land surface in drought each month. Drought is defined as extreme, severe, or moderate, which represents 1%, 5%, and 20%, respectively, of the land surface in drought under present-day conditions. In each case results from the three simulations made using the A2 emissions scenario are shown.

drought the number of events remains stable. There is a significant increase in the mean event duration for all forms of drought.

5. Conclusions

This paper assesses the ability of the Hadley Centre's climate model to reproduce observed changes in drought since 1952 as measured by the Palmer Drought Severity Index (PDSI), the cause of recent global mean decreases in PDSI and to investigate future drought conditions under a realistic emissions scenario.

On a global basis, at time scales between 18 months and 8 yr, the dominant modes of observed and modeled variability are highly correlated with each other both spatially and temporally. In addition, the observed correlation between the 6-month time-lagged Niño-34 index time series and the first principal component of the PDSI is well captured by the model. This observed teleconnection between drought and ENSO events has been well documented (e.g., Ropelewski and Halpert 1987; Shabbar and Skinner 2004; Dai et al. 2004; Barlow et al. 2001).

At time scales greater than 8 yr, there has been a decrease in the global average PDSI of 0.29 decade^{-1}.

The climate models used here, driven by all known twentieth-century external forcings, reproduce this trend, which falls outside the natural variability of the 2000-yr control simulation for nearly all model simulations. An optimal detection analysis demonstrates that there is a detectible contribution from anthropogenic emissions of greenhouse gasses and sulphate aerosols in the production of this drying trend. There are differences between the observed and modeled spatial patterns of wetting and drying. Some of these regional differences are suggested to be a result of natural variability. The rest may be some combination of errors in the large-scale flow of the global model and a poor representation of regional processes and feedbacks in the climate model. Errors introduced by the low resolution of the model will be assessed in the future by the use of regional climate models over relevant areas.

Projections of the global average PDSI under future climate scenarios show a decrease of approximately 0.30 decade^{-1} over the first half of the twenty-first century increasing in magnitude to approximately 0.56 decade^{-1} over the second half of the twenty-first century. In addition, the model predicts a very large increase in the proportion of the land surface under drought by 2090. On a global basis, drought events are slightly

TABLE 1. The mean number of events per 100 yr and the mean event duration over land for extreme, severe, and moderate drought.

Drought type	Number of events per hundred years Mean (standard deviation)			Event duration (month) Mean (standard deviation)		
	ALL-A	2005–50	2050–2100	ALL-A	2005–50	2050–2100
Extreme	5.1 (0.1)	7.5 (0.2)	9.4 (0.2)	12.3 (0.2)	25.5 (1.2)	77.6 (5.5)
Severe	5.8 (0.2)	8.9 (0.2)	9.6 (0.2)	16.4 (0.5)	33.3 (0.1)	97.6 (6.6)
Moderate	9.8 (0.1)	10.5 (0.1)	9.5 (0.4)	27.3 (0.3)	56.1 (1.2)	135.3 (10.8)

more frequent and of much longer duration by the second half of the twenty-first century relative to the present day. Such dramatic increases in drought conditions would lead to substantial impacts and present significant adaptation challenges. Therefore, there is a need for these results to be corroborated by other climate models.

REFERENCES

Allen, M. R., and P. A. Stott, 2003: Estimating signal amplitudes in optimal fingerprinting. Part I: Theory. *Climate Dyn.,* **21,** 477–491.

Alley, W. M., 1984: The Palmer Drought Severity Index: Limitations and assumptions. *J. Climate Appl. Meteor.,* **23,** 1100–1109.

Barlow, M., S. Nigam, and E. H. Berbery, 2001: ENSO, Pacific decadal variability, and U.S. summertime precipitation, drought and streamflow. *J. Climate,* **14,** 2105–2128.

Cook, E. R., D. M. Meko, D. W. Stahle, and M. K. Cleaveland, 1999: Drought reconstructions for the continental United States. *J. Climate,* **12,** 1145–1162.

Dai, A., K. E. Trenberth, and T. R. Karl, 1998: Global variations in droughts and wet spells: 1900–1995. *Geophys. Res. Lett.,* **25,** 3367–3370.

——, ——, and T. Qian, 2004: A global data set of Palmer Drought Severity Index for 1870–2002: Relationship with soil moisture and effects of surface warming. *J. Hydrometeor.,* **5,** 1117–1130.

Folland, C. K., J. Shukla, J. Kinter, and M. Rodwell, 2002: The Climate of the Twentieth Century Project. *CLIVAR Exchanges,* Vol. 7, No. 2, International CLIVAR Project Office, Southampton, United Kingdom, 37–39.

Gordon, C., C. Cooper, C. A. Senior, H. Banks, J. M. Gregory, T. C. Johns, J. F. B. Mitchell, and R. A. Wood, 2000: The simulation of SST, sea ice extents and ocean heat transports in a version of the Hadley Centre coupled model without flux adjustments. *Climate Dyn.,* **16,** 147–168.

Gregory, J. M., J. F. B. Mitchell, and A. J. Brady, 1997: Summer drought in northern midlatitudes in a time-dependent CO2 climate experiment. *J. Climate,* **10,** 662–686.

Guttman, N. B., J. R. Wallis, and J. R. M. Hosking, 1992: Spatial comparability of the Palmer Drought Severity Index. *Water Resour. Bull.,* **28,** 1111–1119.

Heim, R. R., 2002: A review of twentieth-century drought indices used in the United States. *Bull. Amer. Meteor. Soc.,* **83,** 1149–1165.

International ad hoc Detection and Attribution Group (IDAG), 2005: Detecting and attributing external influences on the climate system: A review of recent advances. *J. Climate,* **18,** 1291–1314.

Johns, T. C., and Coauthors, 2003: Anthropogenic climate change for 1860 to 2100 simulated with the HadCM3 model under updated emissions scenarios. *Climate Dyn.,* **20,** 1167–1180.

Jones, P. D., M. Hulme, K. R. Briffa, C. G. Jones, J. F. B. Mitchell, and J. M. Murphy, 1996: Summer moisture availability over Europe in the Hadley Centre general circulation model based on the Palmer Drought Severity Index. *Int. J. Climatol.,* **16,** 155–172.

Keyantash, J., and J. A. Dracup, 2002: The quantification of drought: An evaluation of drought indices. *Bull. Amer. Meteor. Soc.,* **83,** 1167–1180.

Lloyd-Hughes, B., and M. A. Saunders, 2002: A drought climatology for Europe. *Int. J. Climatol.,* **22,** 1571–1592.

Lockwood, J. G., 1999: Is potential evapotranspiration and its relationship with actual evapotranspiration sensitive to elevated atmospheric CO2 levels? *Climatic Change,* **41,** 193–212.

Manabe, S., R. T. Wetherald, P. C. D. Milly, T. L. Delworth, and R. J. Stouffer, 2004: Century-scale change in water availability: CO2-quadrupling experiment. *Climatic Change,* **64,** 59–76.

Nakicenovic, N., and Coauthors, 2000: *Special Report on Emissions Scenarios.* Cambridge University Press, 599 pp.

Ntale, H. K., and T. Y. Gan, 2003: Drought indices and their application to East Africa. *Int. J. Climatol.,* **23,** 1335–1357.

Palmer, W. C., 1965: Meteorological drought. U.S. Weather Bureau Research Paper 45, 85 pp. [Available from NOAA Library and Information Services Division, 1315 East-West Highway, Silver Spring, MD 20910.]

Pope, V. D., M. L. Gallani, P. R. Rowntree, and R. A. Stratton, 2000: The impact of new physical parametrizations in the Hadley Centre climate model: HadAM3. *Climate Dyn.,* **16,** 123–146.

Rayner, N. A., D. E. Parker, E. B. Horton, C. K. Folland, L. V. Alexander, D. P. Rowell, E. C. Kent, and A. Kaplan, 2003: Global analyses of sea surface temperature, sea ice, and night marine air temperature since the late nineteenth century. *J. Geophys. Res.,* **108,** 4407, doi:10.1029/2002JD002670.

Rind, D., R. Goldberg, J. Hansen, C. Rosenzweig, and R. Ruedy, 1990: Potential evapotranspiration and the likelihood of future drought. *J. Geophys. Res.,* **95,** 9983–10 004.

Ropelewski, C. F., and M. S. Halpert, 1987: Global and regional scale precipitation patterns associated with the El Nino–Southern Oscillation. *Mon. Wea. Rev.,* **115,** 1606–1626.

Shabbar, A., and W. Skinner, 2004: Summer drought patterns in Canada and the relationship to global sea surface temperatures. *J. Climate,* **17,** 2866–2880.

Shuttleworth, W. J., 1993: Evaporation. *Handbook of Hydrology,* D. R. Maidment, Ed., McGraw-Hill, 4.1–4.53.

Svoboda, M., and Coauthors, 2002: The drought monitor. *Bull. Amer. Meteor. Soc.,* **83,** 1181–1190.

Tett, S. F. B., and Coauthors, 2002: Estimation of natural and anthropogenic contributions to twentieth century temperature change. *J. Geophys. Res.,* **107,** 4306, doi:10.1029/2000JD000028.

Thornthwaite, C. W., 1948: An approach toward a rational classification of climate. *Geogr. Rev.,* **38,** 55–94.

Walraven, R., 1984: Digital filters. *Proc. Digital Equipment User's Society,* Davis, CA, Department of Applied Science, University of California, 23–30.

Webb, R. W., C. E. Rosenzweig, and E. R. Levine, 1993: Specifying land surface characteristics in general circulation models—Soil profile data set and derived water-holding capacities. *Global Biogeochem. Cycles,* **7,** 97–108.

——, ——, and ——, 2000: Global soil texture and derived water-holding capacities (Webb et al.) data set. Oak Ridge National Laboratory Distributed Active Archive Center, Oak Ridge, TN.

Wetherald, R. T., and S. Manabe, 2002: Simulation of hydrologic changes associated with global warming. *J. Geophys. Res.,* **107,** 4379, doi:10.1029/2001JD001195.

Wilhite, D. A., 2000: Drought as a natural hazard: Concepts and definitions. *Drought: A Global Assessment,* D. A. Wilhite, Ed., Routledge, 3–18.

——, and M. H. Glantz, 1985: Understanding the drought phenomenon: The role of definitions. *Water Int.,* **10,** 111–120.

World Meteorological Organization, 1975: Drought and agriculture. WMO Tech. Note 138, Report of the CAgM Working Group on the Assessment of Drought, Geneva, Switzerland, 127 pp.